Enhancing Humanoid Robot Dynamics: An Optimization Framework for Shoulder Base Angle Adjustment

Jiwon Yoon, Sujin Lee, and Yong Seok Ihn *Member, IEEE*

***Abstract*— Optimizing the initial angle of the shoulder's base frame is crucial for defining the workspace and enhancing the manipulation performance of humanoid robotic arms. Previous studies primarily emphasized geometric analyses, neglecting dynamic factors, which limits their practical applicability. This study presents a multi-metric optimization framework to enhance the dynamic performance of humanoid robotic arms by optimizing the shoulder's initial angle. We formulate a cost function that incorporates torque efficiency, energy consumption, and overload ratio, utilizing the differential evolution (DE) algorithm for optimization. Furthermore, to address the limitations of conventional geometric workspace analysis, we introduce the concept of effective workspace, integrating dynamic constraints to quantitatively evaluate the effects of optimized shoulder angles. We validate the proposed framework in a hybrid simulation environment combining MuJoCo and RBDL, using the KIST humanoid and Unitree G1 robotic arms. Experimental results confirm that the optimized shoulder angles enhance torque distribution, expanding the effective workspace by 18.4% and 3.78% for the KIST and Unitree G1 robotic arms, respectively. These findings demonstrate that the proposed optimization framework enhances manipulation and dynamic performance as well as energy efficiency and system reliability, contributing to advancements in humanoid robotic arm design.**

I. INTRODUCTION

Humanoid robots have been specifically designed to replicate human-like mobility and advance dexterous manipulation capabilities [1]. Recent advancements in locomotion technology are exemplified by state-of-the-art humanoid robots such as Atlas [2], Optimus [3], and Figure 02 [4]. These robots exhibit stable walking, obstacle avoidance, jumping, and balance control in complex environments [5]–[7]. However, manipulation remains constrained by hardware limitations that hinder the ability to skillfully handle objects and perform delicate tasks [8].

In the human arm, the shoulder facilitates gross motion, defining the overall workspace and efficiently distributing torques across joints, with a central axis allowing multi-degree-of-freedom (DoF) [9], [10]. Similarly, the robotic shoulder mimics this functionality and establishes a baseline for the robotic arm's manipulation capabilities.

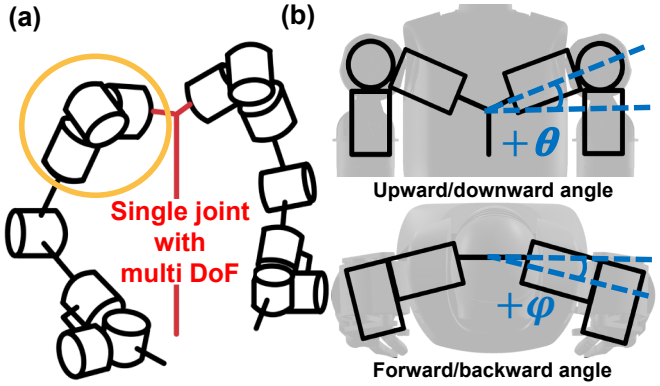

Fig. 1. (a) Design of a robotic arm with a single-joint multiple degrees of freedom shoulder structure, which serves as a baseline for determining the workspace and torque distribution. (b) Influence of scapular movement on upward/downward (θ) and forward/backward (ϕ) angles, demonstrating its significance in optimizing the shoulder base frame orientation.

For example, the robotic shoulder serves as the base frame for the robotic arm, supporting its weight during gross motions. The shoulder's range of motion is critical for determining the arm's workspace and distributing motor torque efficiently across joints [11]. However, increasing payloads significantly limits the stable operational range, causing performance constraints in specific joint configurations [12]. Consequently, even with a sufficient kinematic workspace, the range of feasible movements decreases when manipulating heavier objects. These limitations present significant challenges that prevent humanoid robotic arms from achieving manipulation performance comparable to human arms. One potential approach to address this limitation is modifying the robotic arm's mechanism. However, the design process necessitates a comprehensive evaluation of multiple interrelated parameters, as altering the mechanism alone presents inherent limitations in optimizing overall manipulation capabilities [13].

Given these challenges, deciding the initial angle of the shoulder base frame is crucial for optimizing the manipulation performance of humanoid robotic arms (Fig. 1(a). The initial angle comprises the upward/downward angle (θ) and forward/backward angle (ϕ) (Fig. 1(b)). The WALK-MAN project enhanced the workspace and manipulation capabilities of the robotic arm by adjusting the initial angle of the shoulder base frame [14], [15]. The aforementioned study highlighted that this initial angle is a crucial geometric

This work was supported in part by the National Research Foundation of Korea (NRF) grant funded by the Korean government (MSIT) (No. RS-2024-00464386) and in part by the Korea Institute of Science and Technology (KIST) Institutional Program (No. 2E33601).*(Jiwon Yoon and Sujin Lee contributed equally to this work.) (Corresponding author: Yong Seok Ihn.)*

Jiwon Yoon is with the Center for Humanoid Research, Korea Institute of Science and Technology, Seoul 02792, South Korea, and also with the Department of Mechanical Engineering, Korea University, Seoul 02841, South Korea.

Sujin Lee and Yong Seok Ihn are with the Center for Humanoid Research, Korea Institute of Science and Technology, Seoul 02792, South Korea (e-mail: yongseok.ihn@kist.re.kr).

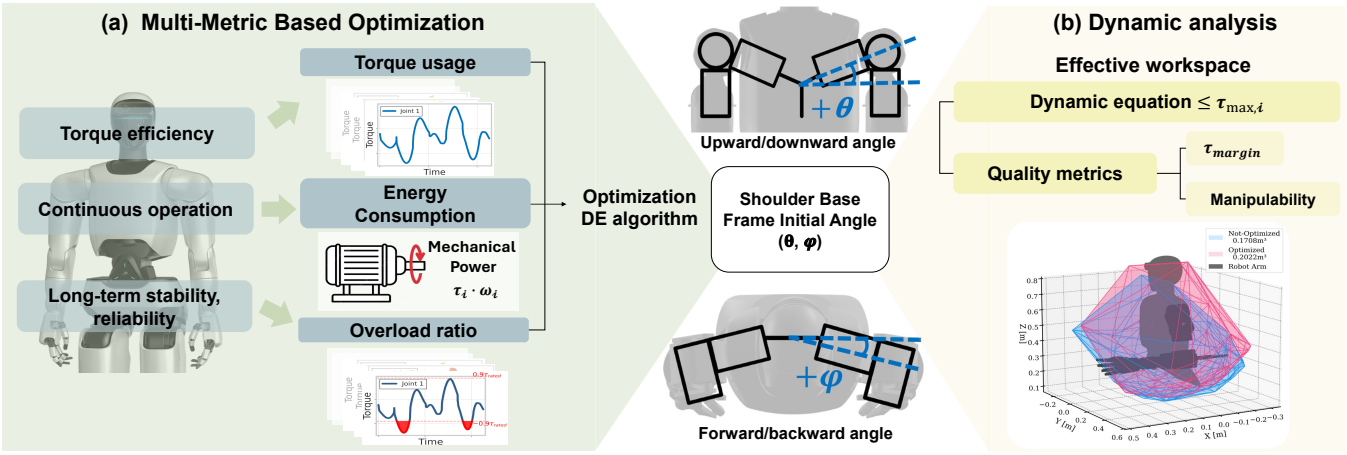

Fig. 2. Multi-metric optimization framework for determining the optimal initial angles for the shoulder base frame. (a) The framework utilizes the differential evolution algorithm to optimize θ,ϕ by evaluating torque usage, energy consumption, and overload ratio, ensuring a balanced dynamic performance. (b) The *effective workspace* concept quantitatively evaluates workspace feasibility by integrating dynamic constraints, addressing the limitations of conventional geometric reachability-based workspace analysis.

parameter and design variable influencing the workspace size and operational efficiency. However, most studies rely on a single kinematic metric to evaluate performance, limiting the comprehensive analysis of the robotic arm's manipulation capabilities. Kinematic analysis alone fails to incorporate various factors present in dynamic environments. Therefore, a multi-metric optimization approach that incorporates various dynamic elements, such as force, torque usage, energy consumption, and motor overload, is necessary.

This study introduces dynamic analysis to optimize the initial angle of the shoulder base frame, expanding the robotic arm's practical workspace and enhancing its manipulation performance. We designed a cost function that integrates torque usage, energy consumption, and overload ratio, systematically including these key dynamic factors in the optimization process. In contrast to conventional geometric reachability-based workspace analyses, the analysis in this study uses the concept of *effective workspace*, which integrates dynamic constraints, such as torque feasibility and manipulability, for a more comprehensive evaluation.

The proposed multi-metric optimization framework (Fig. 2), applied to the G1 (Unitree Robotics) and KIST dual arm, optimizes shoulder base frame angles by integrating torque feasibility and manipulability, enhancing *effective workspace* volume, torque distribution, and operational efficiency for humanoid robotic arm development.

The key contributions of this study are: 1) A multi-metric optimization framework integrating torque efficiency, energy consumption, and overload ratio; 2) Introduction of the effective workspace concept that incorporates dynamic constraints; and 3) Validation of the framework's practical applicability, demonstrating significant workspace expansion and improved manipulation efficiency. The remainder of this paper presents the proposed optimization methodology (Section II), describes the experimental setup (Section III), analyzes optimization results (Section IV), and concludes with findings and future directions (Section V).

II. MULTI-METRIC OPTIMIZATION

Relying on a single performance metric to determine the initial angle of the shoulder base frame is insufficient for real-world applications. A multi-metric optimization approach that integrates multiple factors is essential for deriving an optimal configuration that enhances workspace utilization and manipulation performance. To this end, an optimization framework (Fig. 2) is employed to derive the optimal initial angle of the shoulder base frame using a multi-metric approach.

This section presents the rationale for selecting each performance metric and the basis for assigning weights to each joint [16]. Additionally, a cost function integrating these performance metrics is designed, and a practical criterion, the *effective workspace*, is established to guide the optimization process.

A. Performance Metrics Selection

Optimizing the initial angle of the shoulder base frame necessitates establishing performance indicators that comprehensively address dynamic constraints and operational efficiency.

This study identifies torque usage, energy consumption, and overload ratio as the primary performance indicators for the cost function. Each indicator directly relates to improving the dynamic performance of the design; the physical meaning and weighting rationale are as follows.

1) **Torque usage (C_t)**: Torque usage quantifies the product of the average absolute torque at each joint ($\overline{|\tau_i|}$) and the corresponding weight per joint (μ_i).

$$C_t = \sum_i (\mu_i \cdot \overline{|\tau_i|}) \tag{1}$$

This metric directly reflects the influence of the initial angle of the shoulder base frame on the torque efficiency of the entire system. It aids in identifying the torque

required for specific tasks and is crucial for motor selection and control strategies.

2) **Energy Consumption ($\mathbf{C_e}$)**: Energy consumption is determined by integrating mechanical work, which is calculated as the product of torque and angular velocity at each joint.

$$C_e = \sum_i (\mu_i \cdot \int |\tau_i \cdot \omega_i| \, dt) \tag{2}$$

This metric directly reflects the actual energy used by each joint. For 7-DoF humanoid robots, the energy consumed by each joint in continuous motion is vital for evaluating overall system efficiency and operational endurance [17].

3) **Overload ratio($\mathbf{C_o}$)**: The overload time metric assesses the percentage of time each joint's torque exceeds 90% of its rated torque.

$$C_o = \sum_i \left(\mu_i \cdot \frac{t_{o,i}}{t_{total}} \right) \tag{3}$$

$t_{o,i}$ indicates the duration when $|\tau_i| > 0.9 \cdot |\tau_{rated}|$

Effective overload management in humanoid robot joints significantly influences motor longevity and system reliability [18]. Sustained loads exceeding 90% of the rated torque can degrade motor performance and shorten lifespan, necessitating incorporation into the optimization process for long-term system stability and reliability.

4) **Joint-specific Weight Factors (μ_i)**: Weight distribution μ_i per joint reflects the load carried by each joint during actual work. The shoulder joints ($\mu_{1,2} = 1.0$) supports the load, elbow joints ($\mu_{3,4} = 0.7$) adjust posture, and wrist joints ($\mu_{5,6,7} = 0.5$) facilitate fine coordination [19].

5) **Integrated Cost Function**: Each indicator undergoes min-max normalization before integration to ensure fair comparison and integration of various performance metrics:

$$\hat{C}_t = \frac{C_t - C_{t,min}}{C_{t,max} - C_{t,min}}$$
$$\hat{C}_e = \frac{C_e - C_{e,min}}{C_{e,max} - C_{e,min}}$$
$$\hat{C}_o = \frac{C_o - C_{o,min}}{C_{o,max} - C_{o,min}}$$

The final cost function integrating the three metrics is formulated as

$$C = w_1 \cdot \hat{C}_t + w_2 \cdot \hat{C}_e + w_3 \cdot \hat{C}_o \tag{4}$$

$$\theta \in [-20^\circ, 20^\circ], \quad \phi \in [-20^\circ, 20^\circ], \quad \tau \leq 1.5 \cdot \tau_{\text{rated}}$$

where θ and ϕ represent the rotation angles about the X- and Z-axes, respectively. Coefficients w_1, w_2, and w_3 denote the weighting factors for torque usage, energy consumption, and overload indices, respectively.

Population Size	30	**Mutation Coefficient**	0.8
Max Iterations	2000	**Convergence Tolerance**	0.01
Crossover Rate	0.7	**Mutation Strategy**	Best1bin

TABLE I

PARAMETER SETTINGS FOR THE DIFFERENTIAL EVOLUTION ALGORITHM

Given that the torque usage and overload indices significantly impact performance metrics, including task execution capability, system stability, and motor longevity, these factors are assigned equal weightings of $w_1 = w_3 = 0.35$. Although important for operational efficiency, the energy consumption index has a comparatively lower impact on immediate system performance and is therefore weighted at $w_2 = 0.3$.

B. Optimization

Optimizing the initial angle of the shoulder base frame presents unique challenges due to motor operation characteristics and cost function design. Specifically, torque values may exhibit discontinuities and sudden jumps during motor operation, creating a non-smooth optimization landscape. Additionally, while the cost function captures essential performance metrics, its low dimensionality can lead to local optima in the solution space. To address these challenges, we employed the differential evolution (DE) algorithm [20].

For optimization, we used the mutation operator defined in Eq. (5):

$$V = x_{\text{best}} + F \cdot (x_{r1} - x_{r2}) \tag{5}$$

Here, x_{best} represents the current best solution, F is the mutation coefficient, and x_{r1} and x_{r2} are randomly selected individuals. The parameters were set as shown in Table I, considering the problem characteristics and computational efficiency. Specifically, the crossover rate and mutation coefficient were selected to balance global exploration and local exploitation [21].

To ensure the robustness of the optimization process, the procedure was repeated 20 times. If consistent convergence was observed, the solution was considered the optimal shoulder angle. This indicates that the proposed optimization approach provides stable and reliable solutions.

During the optimization process, the previously defined cost function was used as the objective function, and the following steps were performed in each iteration:

1) **Initialization:** A population of candidate solutions was generated by randomly assigning values to θ and ϕ within the range of $[-20^\circ, 20^\circ]$.
2) **Mutation:** New candidate solutions were created using the mutation operator in Eq. (5).
3) **Crossover:** A binary crossover operation was applied to generate new offspring.
4) **Selection:** The best solutions were selected based on their cost function values.
5) **Termination Check:** The process terminated either when the maximum number of iterations was reached or when the convergence criterion was met.

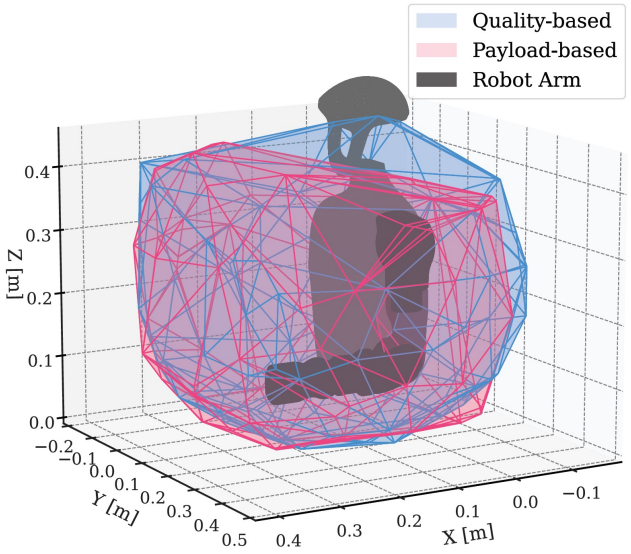

Fig. 3. 3D workspace comparison between quality-based (*effective workspace*) and payload-based workspace with the robot model. Quality-based workspace represents regions where the quality metric exceeds a predefined threshold, while payload-based workspace indicates regions where the robot can operate successfully with a 5 kg payload, considering torque constraints. The humanoid robot arm is visualized at the center of the workspace for reference.

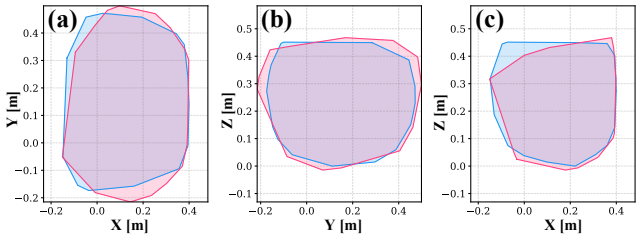

Fig. 4. 2D workspace projections of Fig. 3 comparing quality-based (*effective workspace)* and payload-based workspace: (a) XY, (b) YZ, and (c) XZ projections.

This systematic approach enabled efficient exploration of the solution space while ensuring convergence to an optimal configuration. The optimization results were experimentally verified (Section IV).

C. Evaluation method

The performance evaluation of the optimized initial angle of the shoulder base frame requires consideration of the dynamic aspects, particularly for practical applications. Although a position might be kinematically reachable, it can become infeasible if the required torque exceeds the motor's capability under a load. Previous studies have focused on geometric workspace analysis through joint range of motion. In contrast, this study proposes the concept of *effective workspace*, which incorporates dynamic constraints to determine optimal shoulder angles for real-world applications. The *effective workspace* is defined as

$$\textit{Effective Workspace Volume: } V(W_{eff}) \tag{6}$$

$$W_{eff} = \left\{ \mathbf{x} \in R^3 | Q(\mathbf{x}) \geq Q_{min}, x = f(q), \tau(q, \dot{q}, \ddot{q}) \leq \tau_{\max} \right\} \tag{7}$$

where W_{eff} represents the effective workspace that incorporates the dynamic constraints. It is defined as the set of coordinates that satisfy the equations of motion and a minimum quality threshold Q_{min}. The dynamic constraints for each joint are expressed as

$$\tau_i(q, \dot{q}, \ddot{q}) = M_i(q)\ddot{q} + C_i(q, \dot{q})\dot{q} + G_i(q) \leq \tau_{\max,i} \quad \forall i \in 1, \ldots, 7 \tag{8}$$

Here, $M_i(q)$ represents the inertia matrix, $C_i(q, \dot{q})$ denotes the Coriolis and centrifugal terms, and $G_i(q)$ accounts for the gravitational effects. The quality metric is defined as

$$Q(\mathbf{x}) = \alpha \frac{w(\mathbf{x})}{w_{max}} + (1 - \alpha)\tau_{margin} \tag{9}$$

The manipulability index $w(x)$ is computed using the Jacobian matrix, which relates end-effector velocities to joint velocities, serving as a measure of dexterity at a given position. The manipulability index and torque margin are defined as

$$w(x) = \sqrt{\det(JJ^T)} \tag{10}$$

$$\tau_{margin} = \min_{i=1,\ldots,7} \tau_{margin,i} \; \tau_{margin,i} = 1 - \frac{|\tau_i|}{\tau_{rated,i}} \tag{11}$$

The evaluation methodology facilitates a thorough analysis of the impact of optimizing the initial angle of the shoulder base frame on task execution dynamically. To validate that the *effective workspace* appropriately captures dynamic constraints, we compared the workspace obtained from filtering a no-payload workspace using Q_{min} with that obtained under a 5 kg payload condition. The optimization aimed to find parameter combinations that yield *effective workspace* volumes closely matching those of the 5 kg payload workspace, ensuring that the quality-based filtering method effectively represents dynamically feasible regions. We conducted an iterative optimization process to identify key parameters in the equation development. Specifically, we performed a grid search with α constrained between [0,1] in 0.01 increments. For each parameter combination, we varied the threshold Q_{min} from 0.3 to 0.9 in 0.001 increments to calculate the *effective workspace* volume. The optimal performance was achieved with

- $\alpha = 0.45$
- Optimal quality threshold $Q_{min} = 0.752$

We confirmed the validity of these parameter settings through comprehensive 2D and 3D workspace distribution analysis (Figs. 3 and 4). The key findings are as follows:

- Quality function-based workspace volume: 0.0952 m³
- Payload-based workspace volume: 0.0942 m³
- Overlap volume between workspaces: 0.0870 m³
- Spatial correlation: 91.7

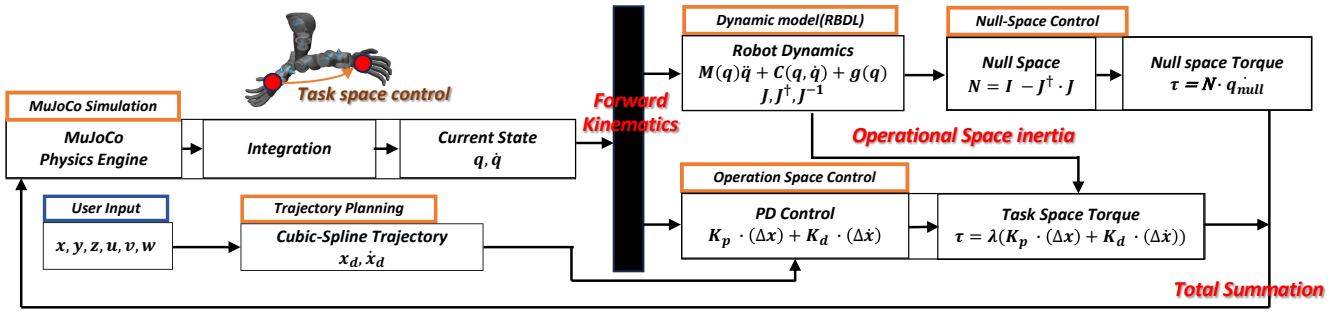

Fig. 5. Proportional-Derivative (PD) and Null-Space control system for the 7-DOF robotic manipulator in the MuJoCo-RBDL hybrid simulation environment. PD control regulates primary task-space motion, while Null-Space control optimally utilizes redundant degrees of freedom. The total control torque (τ_{total}) prioritizes shoulder torque allocation, leveraging its higher capacity to enhance load distribution and motor efficiency in humanoid applications.

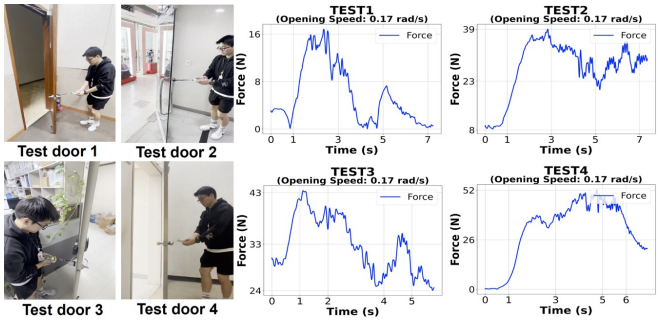

Fig. 6. Experimental results of torque measurement during the door-opening task. The peak torque values remained just below 50N · m across all tested conditions, confirming the torque requirements for stable door operation.

An even higher correlation rate can be anticipated when considering the actual operational space of the end-effector. The 2D projections demonstrated strong similarities in spatial distribution patterns across the XY, YZ, and XZ planes. This substantial overlap validates that the proposed quality function effectively predicts the actual workspace under load conditions.

Using this validation methodology, Section IV presents comprehensive performance evaluations of our humanoid robotic arm and Unitree G1, demonstrating the practical applicability of the proposed optimization framework.

III. EXPERIMENT ENVIRONMENTS

A. Hybrid Simulation Environments

We developed a hybrid simulation that integrates MuJoCo for physics-based dynamics and RBDL for inverse kinematics to optimize the initial angle of the shoulder base frame. MuJoCo ensures accurate contact dynamics, while RBDL supports dynamic calculations, leveraging both tools' strengths.

1) Kinematic Configuration
The robot has a 7-DoF kinematic structure, comprising a 3-DoF shoulder, 1-DoF elbow, and 3-DoF wrist. We define two rotation angles (θ, ϕ) as design variables to evaluate the impact of the shoulder base frame on system performance (Fig. 1(a)).
2) Model Conversion and Generation
MJCF and URDF formats of the robot model were complementarily utilized for a comprehensive motion analysis of the system. Considering the differences in Euler angle representations between the two file formats, we generated 81 distinct shoulder configurations by varying the θ and ϕ rotations from $-20°$ to $-20°$ in $5°$ increments.
3) Door-Opening Task
Door handles are among the most standardized designs in human environments, rendering them suitable for evaluating key performance metrics such as robot arm speed, force manipulability, and joint rotation range. Additionally, the ability to easily adjust parameters during evaluation makes door-opening tasks ideal for dynamic optimization. Therefore, this study focuses on dynamically optimizing shoulder joint angles using door-opening motions.
Experiments were conducted on four commonly used door types in real-world settings. Fig. 6 presents the experimental setup and the measured force–time graph. The experiments were conducted at 0.17 and 0.21 rad/s [22], reflecting average human door-opening speeds from previous studies. A maximum force of 50 N was recorded at these speeds. Accordingly, the 7-DoF robotic manipulator was optimized to withstand a force of 50 N.

B. Control Systems

In this study, workspace control was implemented to effectively manage the 7-DoF robotic manipulator. The primary task within the workspace follows a proportional-derivative (PD) control, as described in Eq. (12). Fig. 5 illustrates that the proposed system uses null-space control, leveraging redundant DoF to achieve additional control objectives while performing primary tasks [23].

$$\tau_{\text{PD}} = J^{\dagger} \cdot \lambda \cdot (K_p \cdot q + K_d \cdot \dot{q}) + g(q), \tag{12}$$

$$\tau_{\text{null}} = w \cdot \left(I - J^{\dagger} \lambda M^{-1}\right)\left(K_n \cdot \dot{q}\right), \tag{13}$$

$$\tau_{\text{total}} = \tau_{\text{PD}} + \tau_{\text{null}}. \tag{14}$$

In Eqs. (12) and (13), λ and M represent the operational space and inertia matrices of the robot, respectively. The

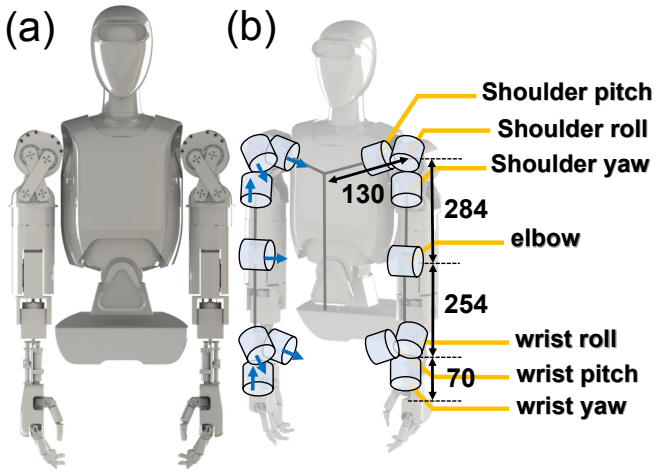

Fig. 7. 3D CAD and DH parameters of the KIST arm

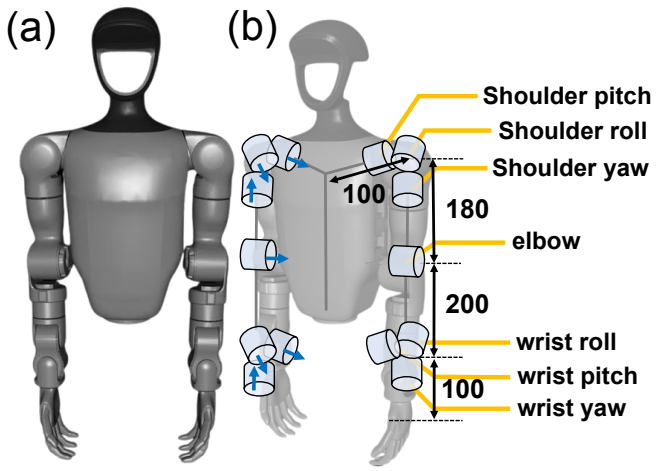

Fig. 8. 3D CAD and DH parameters of the Unitree G1 arm

TABLE II
SPECIFICATIONS OF KIST ARM

Items	Specifications
Size and Shape	7-DoF per arm - Shoulder 3-DoF, elbow 1-DoF, wrist 3-DoF
Mass	Arm moving part: 8.6 kg
Range of motion (left arm)	Shoulder pitch: -180° $\sim$ 180° Shoulder roll: -125° $\sim$ 95° Shoulder yaw: -180° $\sim$ 180° Elbow: -180° $\sim$ 0° Wrist roll, pitch: -45° $\sim$ 45° Wrist yaw: -180° $\sim$ 180°
Speed	Shoulder roll, pitch: 144 deg/s Shoulder yaw: 654 deg/s Elbow: 654 deg/s Wrist roll, pitch: 16,556 deg/s(with 6mm ballscrew) Wrist yaw: 720 deg/s

TABLE III
SPECIFICATIONS OF UNITREE G1

Items	Specifications
Size and Shape	7-DoF per arm - Shoulder 3-DoF, elbow 1-DoF, wrist 3-DoF
Mass	Arm moving part: 3.63 kg
Range of motion (left arm)	Shoulder pitch: -177° $\sim$ 153° Shoulder roll: -90° $\sim$ 129° Shoulder yaw: -150° $\sim$ 150° Elbow: -60° $\sim$ 120° Wrist roll: -113° $\sim$ 113° Wrist yaw, pitch: -90° $\sim$ 90°
Speed	Shoulder roll, pitch: 540 deg/s Shoulder yaw: 540 deg/s Elbow: 540 deg/s Wrist roll: 630 deg/s Wrist yaw, pitch: 630 deg/s

pseudo-inverse of the Jacobian matrix $J^{\dagger}$ maps task-space forces to joint torques, using diagonal gain matrices K_p, K_d, and K_n. Joint-specific weights(w) account for varying torque capacities, enhancing energy efficiency by optimizing load distribution, particularly by leveraging the shoulder joints' high torque capacities.

The controller's reliability was validated by analyzing changes in the Jacobian matrix due to modifications in the shoulder coordinate system, ensuring that the end-effector consistently reached the target position across all configurations.

IV. EXPERIMENTAL VALIDATION OF THE OPTIMIZATION FRAMEWORK

This section describes the implementation and evaluation of the proposed optimization framework for the KIST humanoid and Unitree G1 robot arms. The angles θ and ϕ were optimized to minimize torque usage, energy consumption, and overload ratio while maximizing the *effective workspace*. The optimization employed a multi-metric approach using the DE algorithm. To validate the optimization results, we generated 2D heatmaps for each performance metric, illustrating the distribution of torque, energy consumption, overload ratio, and total cost function across varying initial angles of the shoulder base frame.

A. KIST ARM

The final optimized joint angles for the KIST arm were determined as

- Optimal θ = 13.3°
- Optimal ϕ = 3.1°

The normalized torque usage distribution highlights an optimal low-torque region between $\theta = 7°$ to $15°$ and $\phi = -2°$ to $5°$, indicating a more balanced load distribution across the system (Fig. 9(b)). The normalized energy consumption heatmap reveals that energy efficiency is maximized within $\theta = 8°$ to $17°$ and $\phi = -1°$ to $6°$, where energy consumption is its lowest (Fig. 10(a)). The normalized overload ratio follows a similar pattern, with minimal overload in the range $\theta = 9°$ to $16°$ and $\phi = 0°$ to $7°$, with significant increases for $\theta > 18°$ (Fig. 10(b)). Lastly, the total cost function suggests that the optimal trade-off among energy, torque, and overload is found within $\theta = 10°$ to $15°$ and $\phi = 0°$ to $4°$, closely aligning with the optimized angles. Moreover, the

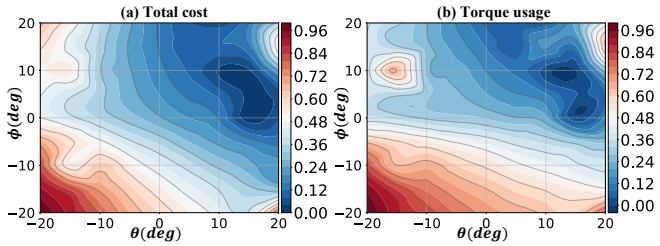

Fig. 9. Elements for evaluating optimization of KIST arm. (a) total cost of θ-ϕ plane and (b) torque usage of θ-ϕ plane

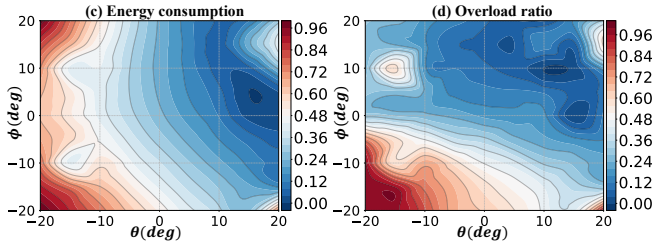

Fig. 10. Elements for evaluating optimization of KIST arm: (a) energy consumption of θ-ϕ plane and (b) overload ratio of θ-ϕ plane

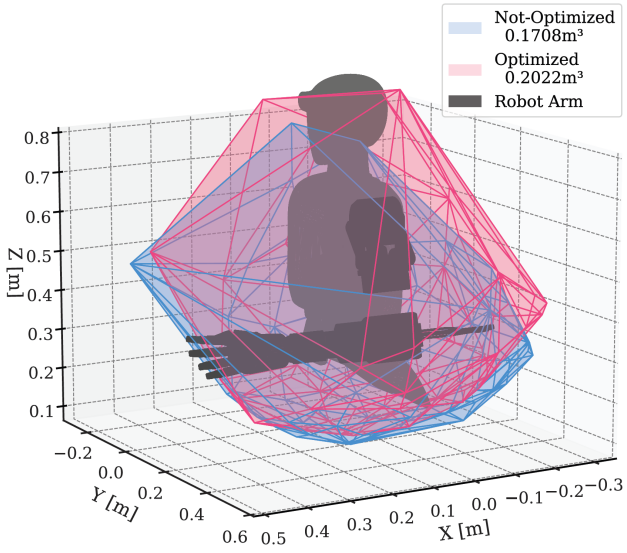

Fig. 11. *Effective workspace* comparison between optimized and non-optimized KIST robot arm.

effective workspace analysis demonstrated an expansion from $0.1708\,m^3$ to $0.2022\,m^3$, representing approximately 18.4% increase, which enhances task flexibility and operational reach.

B. Unitree G1 ARM

The final optimized joint angles for the Unitree G1 Arm were determined as

- Optimal θ = 14.4°
- Optimal ϕ = 2.4°

The normalized torque usage distribution shows an optimal low-torque region between $\theta = 9°$ to $16°$ and $\phi = -2°$ to $6°$, where motor loads balance evenly (Fig. 12(b)). The normalized energy consumption heatmap indicates that energy efficiency peaks between $\theta = 10°$ to $18°$ and $\phi = 0°$ to $5°$, with the lowest values appearing in this range (Fig. 13(a)). The normalized overload ratio exhibits a similar trend, with minimal overload around $\theta = 10°$ to $17°$ and $\phi = 0°$ to $6°$, while higher overload values occur beyond $\theta = 20°$ (Fig. 13(b)). Finally, the total cost function reveals that the best balance of energy, torque, and overload occurs within $\theta = 12°$ to $16°$ and $\phi = 0°$ to $4°$, confirming that the optimized angles fall within this favorable region. Furthermore, the *effective workspace* analysis indicates a significant volume expansion from $0.0952\,m^3$ to $0.0988\,m^3$, an increase of approximately 3.78%, enhancing the robot's reachability and task flexibility.

V. CONCLUSION

This study presents a multi-faceted optimization approach for the initial angle of the shoulder base frame in a 7-DoF humanoid robotic arm to enhance its dynamic performance. In contrast to traditional geometric analyses, we introduced a kinematic–dynamic optimization framework that incorporates torque efficiency, energy consumption, and overload ratio for a comprehensive performance evaluation. In addition, the DE algorithm was employed to identify optimal shoulder angles, validated through hybrid simulations and real-world robotic experiments. Furthermore, an *effective workspace* was introduced as a practical metric for evaluating these optimized configurations. The experiments demonstrated an 18.4% and 3.78% expansion in the *effective workspace* for the KIST and Unitree G1 robot arms, respectively, confirming improvements in manipulation efficiency, torque distribution, and task performance.

This work bridges the gap between geometric feasibility and dynamic efficiency in humanoid robot design. By refining workspace evaluation methods and incorporating multi-metric optimization, it lays the foundation for adaptive, high-performance robotic systems capable of efficient manipulation and task flexibility in real-world scenarios.

Our approach significantly contributes to humanoid robotics as it fills the gap in traditional geometric workspace evaluations by factoring in dynamic factors such as torque usage, energy efficiency, and overload management, offering a more reliable optimization method. Additionally, the *effective workspace* (W_{eff}) offers a standardized framework for comparing real-world performances across different robotic platforms.

Moving forward, we aim to extend this framework to more complex task scenarios. Future work will focus on integrating learning-based motion planning to derive global shoulder angle solutions that adapt to various tasks and incorporate real-time dynamic constraints. We also plan to compare our dynamic optimization with traditional kinematic methods, demonstrating that our approach yields more effective workspaces and higher operational efficiency. While the framework has been primarily tested through simulations,

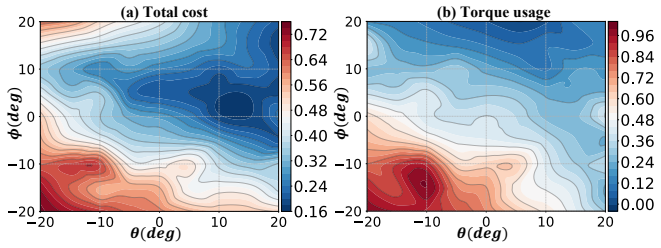

Fig. 12. Elements for evaluating optimization of G1 arm: (a) total cost of θ-ϕ plane and (b) torque usage of θ-ϕ plane

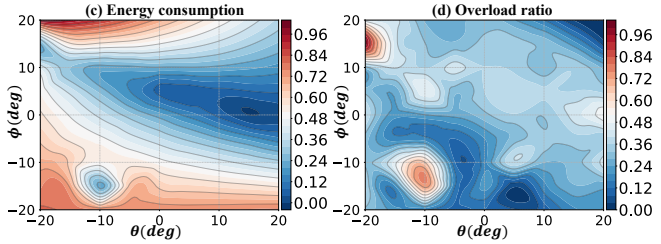

Fig. 13. Elements for evaluating optimization of G1 arm. (a) energy consumption of θ-ϕ plane and (b) overload ratio of θ-ϕ plane

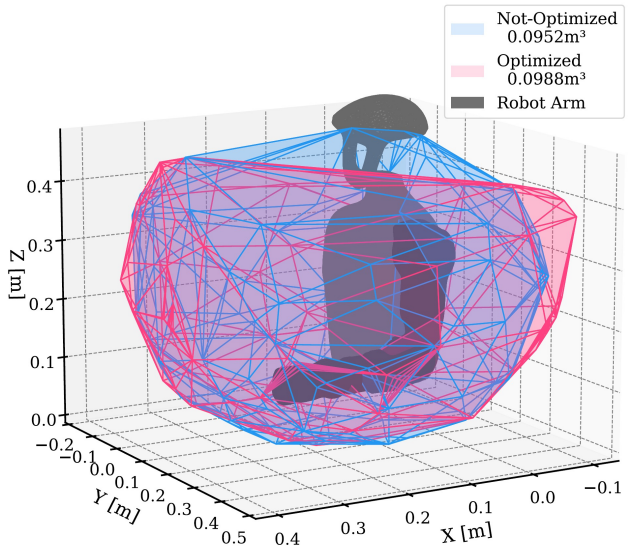

Fig. 14. *Effective workspace* comparison between optimized and non-optimized G1 robot arm.

further evaluations in real-world systems will validate its practical utility in enhancing humanoid robot capabilities.

REFERENCES

[1] A. Billard and D. Kragic, "Trends and challenges in robot manipulation," *Science*, vol. 364, no. 6446, p. eaat8414, 2019.

[2] B. Dynamics, "Atlas: The world's most dynamic humanoid robot," 2023, accessed: 2025-02-19. [Online]. Available: https://www.bostondynamics.com/atlas

[3] I. Tesla, "Tesla unveils optimus gen 2: Advancements in humanoid robotics," 2024, accessed: 2025-02-19. [Online]. Available: https://www.tesla.com/AI

[4] Tesla, "Tesla optimus gen 2: Official demonstration," February 2024, accessed: 2025-02-19. [Online]. Available: https://www.youtube.com/watch?v=0SRVJaOg9Co

[5] M. A. Hopkins, D. W. Hong, and A. Leonessa, "Humanoid locomotion on uneven terrain using the time-varying divergent component of motion," in *2014 ieee-ras international conference on humanoid robots*. IEEE, 2014, pp. 266–272.

[6] M. F. Fallon, P. Marion, R. Deits, T. Whelan, M. Antone, J. McDonald, and R. Tedrake, "Continuous humanoid locomotion over uneven terrain using stereo fusion," in *2015 IEEE-RAS 15th International Conference on Humanoid Robots (Humanoids)*. IEEE, 2015, pp. 881–888.

[7] Y. Tong, H. Liu, and Z. Zhang, "Advancements in humanoid robots: A comprehensive review and future prospects," *IEEE/CAA Journal of Automatica Sinica*, vol. 11, no. 2, pp. 301–328, 2024.

[8] T. Asfour, P. Azad, N. Vahrenkamp, K. Regenstein, A. Bierbaum, K. Welke, J. Schroeder, and R. Dillmann, "Toward humanoid manipulation in human-centred environments," *Robotics and Autonomous Systems*, vol. 56, no. 1, pp. 54–65, 2008.

[9] G. Gulletta, W. Erlhagen, and E. Bicho, "Human-like arm motion generation: A review," *Robotics*, vol. 9, no. 4, p. 102, 2020.

[10] B. Kim and A. D. Deshpande, "An upper-body rehabilitation exoskeleton harmony with an anatomical shoulder mechanism: Design, modeling, control, and performance evaluation," *The International Journal of Robotics Research*, vol. 36, no. 4, pp. 414–435, 2017.

[11] W. Li, Y. Wang, S. Togo, H. Yokoi, and Y. Jiang, "Development of a humanoid shoulder based on 3-motor 3 degrees-of-freedom coupled tendon-driven joint module," *IEEE Robotics and Automation Letters*, vol. 6, no. 2, pp. 1105–1111, 2021.

[12] C. Sartore, L. Rapetti, and D. Pucci, "Optimization of humanoid robot designs for human-robot ergonomic payload lifting," in *2022 IEEE-RAS 21st International Conference on Humanoid Robots (Humanoids)*. IEEE, 2022, pp. 722–729.

[13] J. K. Paik, B. H. Shin, Y.-b. Bang, and Y.-B. Shim, "Development of an anthropomorphic robotic arm and hand for interactive humanoids," *Journal of bionic engineering*, vol. 9, no. 2, pp. 133–142, 2012.

[14] M. Bagheri, A. Ajoudani, J. Lee, D. G. Caldwell, and N. G. Tsagarakis, "Kinematic analysis and design considerations for optimal base frame arrangement of humanoid shoulders," in *2015 IEEE international conference on robotics and automation (ICRA)*. IEEE, 2015, pp. 2710–2715.

[15] N. G. Tsagarakis, D. G. Caldwell, F. Negrello, W. Choi, L. Baccelliere, V.-G. Loc, J. Noorden, L. Muratore, A. Margan, A. Cardellino *et al.*, "Walk-man: A high-performance humanoid platform for realistic environments," *Journal of Field Robotics*, vol. 34, no. 7, pp. 1225–1259, 2017.

[16] A. Pérez-González, V. Roda-Casanova, and J. Sabater-Gazulla, "Predicting wrist joint angles from the kinematics of the arm: Application to the control of upper limb prostheses," *Biomimetics*, vol. 8, no. 2, p. 219, 2023.

[17] W. Kong, J. Wang, D. Kong, Y. Cong, and S. Feng, "Motor shifting and torque distribution control of a multi-motor driving system in electric construction vehicles," *Advances in Mechanical Engineering*, vol. 13, no. 6, p. 16878140211028446, 2021.

[18] H. Zhao, L. Bo, C. Peng, W. Gu, P. Wang, and B. Chen, "Integrated torque sensors for humanoid robot joints," in *Journal of Physics: Conference Series*, vol. 2815, no. 1. IOP Publishing, 2024, p. 012017.

[19] A. Hazari, A. G. Maiya, T. V. Nagda, A. Hazari, A. G. Maiya, and T. V. Nagda, "Lever systems at human joints and muscles," *Conceptual Biomechanics and Kinesiology*, pp. 53–57, 2021.

[20] K. Ushiyama, S. Sato, and T. Matsuo, "A unified discretization framework for differential equation approach with lyapunov arguments for convex optimization," *Advances in Neural Information Processing Systems*, vol. 36, pp. 26 092–26 120, 2023.

[21] F. Fröhlich and P. K. Sorger, "Fides: Reliable trust-region optimization for parameter estimation of ordinary differential equation models," *PLoS computational biology*, vol. 18, no. 7, p. e1010322, 2022.

[22] S.-B. Wang and C.-F. Wu, "Design of the force measuring system for the hinged door: Analysis of the required operating torque," *International Journal of Industrial Ergonomics*, vol. 49, pp. 1–10, 2015.

[23] H. Sadeghian, L. Villani, M. Keshmiri, and B. Siciliano, "Task-space control of robot manipulators with null-space compliance," *IEEE Transactions on Robotics*, vol. 30, no. 2, pp. 493–506, 2013.